Methods for Attenuating and Terminating Waves in Ridge Gap Waveguide at W_Band Carbon-Loaded Foam Carbonyl Iron Paint and Nickel Plating

Methods for Attenuating and Terminating Waves in Ridge Gap Waveguide at W-Band: Carbon-Loaded Foam, Carbonyl Iron Paint, and Nickel Plating

Artem R. Vilenskiy, Yingqi Zhang, Marianna V. Ivashina
Antenna Group, Dept. of Electrical Engineering, Chalmers University of Technology, 41296 Gothenburg, Sweden,
artem.vilenskiy@chalmers.se

***Abstract*— Several methods for electromagnetic waves matched termination and attenuation in a ridge gap waveguide (RGW) are experimentally investigated at W-band. At these frequencies, the implementation of matched loads and attenuators is especially complicated due to small sizes of RGW design features that limits application of traditional waveguide absorbing structures (e.g., absorbing sheets and finlines, ferrite insets, carbonyl iron walls, etc.). The following three techniques are considered: (i) filling an RGW gap with a carbon-loaded foam; (ii) covering a ridge (and pins) with a carbonyl iron paint; (iii) selective nickel plating of an RGW line segment. It was found that the first method exhibits a great broadband absorbing performance and can be easily implemented in a lab environment, whereas the second method can realize a more accurate and predictable attenuating performance. Finally, nickel plating allows for designing resonant RGW terminations and is more interesting from the industrial perspective.**

***Keywords*— ridge gap waveguide, matched termination, carbon-loaded foam, carbonyl iron, nickel plating.**

I. Introduction

Gap waveguide (GWG) technology has attracted a lot of interest recently being applied in the areas of antenna and microwave circuits design [1], [2]. The contactless GWG structure greatly alleviates manufacturing accuracy requirements as compared with classical hollow metal waveguide designs. This advantage is especially important at high millimeter(mm)-wave frequencies (W- and D-band) where existing manufacturing technologies almost reached their accuracy limits [3]. Likely, the ridge gap waveguide (RGW) is the most widely used GWG component owing to its relatively compact transverse sizes and wideband single-mode operation [4]. The RGW has been utilized in various mm-wave devices [1], [2], [5] such as array antennas, power distribution networks, filters, couplers, etc. On another note, many traditional waveguide components are yet to be developed in the RGW technology. This, e.g., is related to RGW attenuators and matched terminations (loads) that, to the authors' knowledge, thus far have not been reported. There is a great practical need in this type of devices for termination of multi-port mm-wave circuits. That includes design of RGW directional couplers and circulators, array antenna laboratorial measurements, and many other applications.

Conventional microwave and mm-wave waveguide loads employ different absorbing insets such as resistive sheets [6], ferrites [7], carbonyl iron blocks [8], etc. In most cases, these elements are precisely located in the waveguide with a proper impedance matching taper. However, at W-band and higher frequencies, a realization of such designs inside a contactless and physically small RGW becomes either very complicated or even impossible. In this contribution, we report on experimental results of RGW waves attenuation and termination at W-band. A regular RGW is considered as a basic structure that has been differently loaded with several absorbing materials: (i) filled with a carbon-loaded foam; (ii) covered by a carbonyl iron paint; (iii) selectively nickel-plated. The presented initial experimental results allow for formulating design guidelines for future industrial and laboratorial mm-wave RGW matched loads and attenuators.

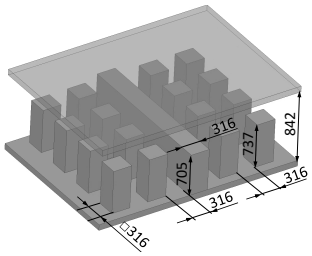

Fig. 1. The basic RGW structure with design dimensions (in μm).

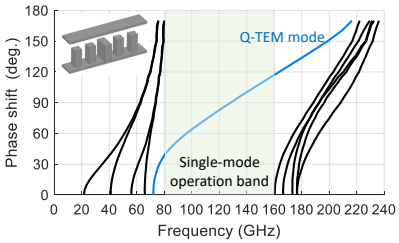

Fig. 2. Dispersion diagram of the basic RGW.

II. Basic RGW and Test Structures

Fig. 1 demonstrates a geometry of the basic RGW used in this study. Two rows of pins are employed at each side of the central ridge, which was found enough to prevent any unwanted mm-wave energy leakage. The RGW dispersion diagram (for a single-period pin structure) is given in Fig. 2 [4]. It can be found that a single quasi-TEM mode operation regime was realized in the (80 – 160) GHz range. At the same

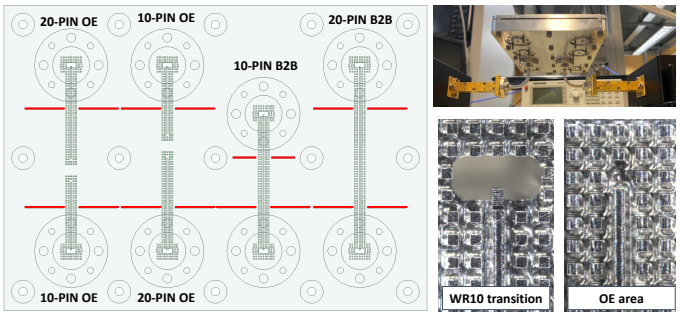

Fig. 3. Geometries of the test RGW designs (left), including 10- and 20-pin back-to-back (B2B) and open-ended (OE) structures (red lines depict positions of the measurement reference planes). The manufactured prototype and the measurement setup (top right). Microscope images of the WR10-to-RGW transition and the OE termination (bottom right).

time, the RGW can be practically used approximately above 82 GHz (the weak-dispersion region).

Four test aluminum RGW designs have been fabricated using CNC milling to study different RGW termination methods. These structures are presented in Fig. 3: 10- and 20-pin back-to-back (B2B) and open-ended (OE) RGWs. All structures are interfaced with the measurement equipment through the standard WR10 waveguides that was realized using a wideband orthogonal WR10-to-RGW transition [9]. In Fig. 3, the red lines indicate the measurement reference planes separating the RGW volume being loaded with different absorbing materials in the following section. In order to exclude the influence of the WR10-to-RGW transitions, a dedicated TRL calibration kit was manufactured and used in measurements. First, all test designs were measured without absorbers. The corresponding results are presented in Fig. 4. As seen, for the B2B designs, some S_{11} peaks reach values above –20 dB. This is due to the limited manufacturing accuracy of the TRL calibration standards. The calibration realizes an acceptable measurement performance above 85 GHz (where the LINE standard provides a sufficient phase delay). In Fig. 4, simulated S_{21} (B2B structures) and S_{11} (OE structures) are presented for comparison. These results were computed in Ansys HFSS using Groisse surface roughness model ($R_q = 0.5$ μm). The measured insertion loss of the basic RGW at 95 GHz is estimated as 0.5 dB/cm.

III. RGWs Loaded with Absorbing Materials

A. Carbon-Loaded Absorbing Foam

To create the first implementation of the matched RGW termination we used a carbon-loaded absorbing foam WAVASORB® FS from Emerson & Cuming. The foam can be classified as a dielectric loss absorbing material, i.e. the electromagnetic energy loss occurs due to a high dielectric loss tangent [10]. At the time of publication, measurements of absorber electromagnetic properties in W-band are ongoing. We used foam patches of approximately 300-μm thickness that were directly inserted into the air gap of the RGW. To improve the impedance matching, the foam patches were

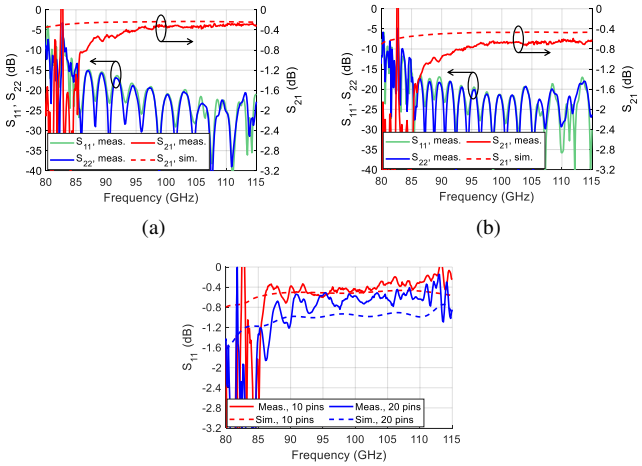

Fig. 4. Measured and simulated S-parameters of the test RGW designs without absorbers: (a) 10-pin B2B structure; (b) 20-pin B2B structure; (c) OE structures.

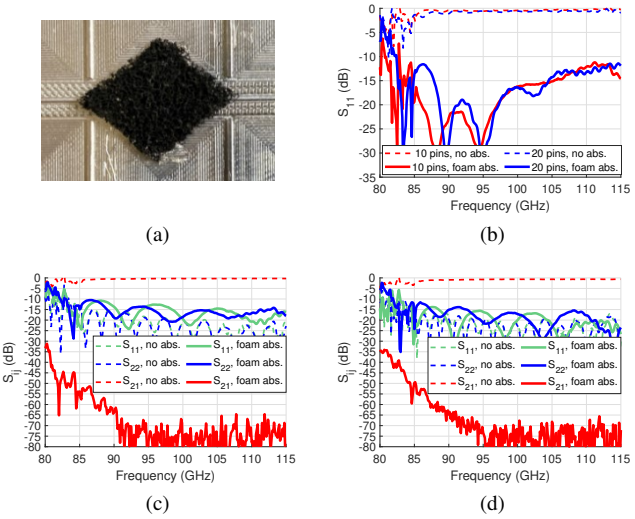

Fig. 5. (a) The H-plane tapered foam absorber inserted into the 10-pin B2B structure. Comparison of measured S-parameters with and without the foam absorber: (b) OE structures; (c) 10-pin B2B structure; (d) 20-pin B2B structure.

tapered in the H-plane with 60 deg. tapering angle, as shown in Fig. 5a. Measured results (Fig. 5) evidence a great absorption performance: measured S_{21} for both 10- and 20-pin B2B structures is below –50 dB for the frequencies above 85 GHz. The foam introduces some impedance mismatch, as can be seen by the increased level of S_{11} and S_{22}. The average mismatch level is –15 dB. The authors have found that the mismatch can be further improved by reducing the foam patch thickness to 150-200 μm and using an additional fixture for an accurate foam mounting. On the other hand, employing the foam absorber for a precise attenuation can be tricky due high loss per unit length and difficulty of controlling the foam patch length.

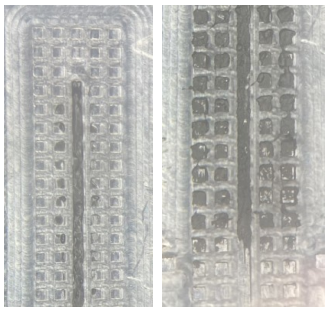

(a)

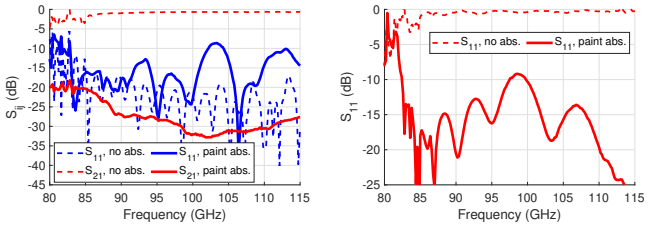

(b) (c)

Fig. 6. (a) The RGW with the carbonyl iron paint covering only the ridge or both the ridge and pins. Comparison of measured S-parameters with and without the paint: (b) 20-pin B2B structure; (c) 20-pin OE structure.

B. Carbonyl Iron Paint

Next, the application of the carbonyl iron paint was investigated. We used the off-the-shelf coated carbonyl iron based paint in urethane acrylic resin MF-500 from MWT Materials Inc. The paint has been characterized up to 20 GHz and no data is available for W-band at the time of publication. In general, carbonyl iron paints at microwave and low mm-wave frequencies demonstrate both dielectric and magnetic absorbing properties [11], [12]. However, taking into account typical complex permeability dispersion curves of carbonyl iron, the authors believe that at W-band the dielectric loss should provide the major contribution to the absorption mechanism.

Several methods of the RGW painting have been tested. First, only ridge was painted, as shown in Fig. 6a. In the second case, both ridge and pins were covered with the paint. The paint thickness is the crucial parameter defining insertion loss per unit length and a quality of impedance matching. Since, the painting was done manually, it was hard to control the thickness precisely. The estimated paint thickness after curing is in the range of 50-70 μm. We have found that covering the pins provides almost no change in the attenuation performance. It was expected since most of the mm-wave field energy is concentrated between the ridge and the top metal plate. Two test structures (20-pin B2B and OE) were painted and measured. The corresponding results are demonstrated in Fig. 6b, 6c. As seen, the paint is capable of realizing a quite strong attenuation – the S_{21} of the B2B structure is below –20 dB. At the same time, it is harder to control impedance matching as compared with the absorbing foam. On the other hand, since the loss per unit length is not as high as for the foam absorber, the paint can also be exploited for a fixed attenuator design. It is believed that using a painting stencil can greatly improve both impedance matching and performance repeatability.

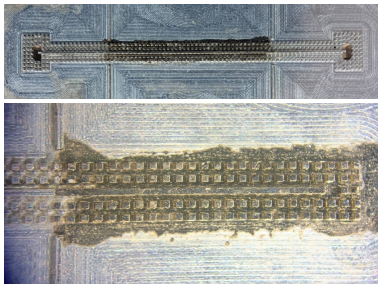

Fig. 7. Photographs of the selectively nickel-plated test structures.

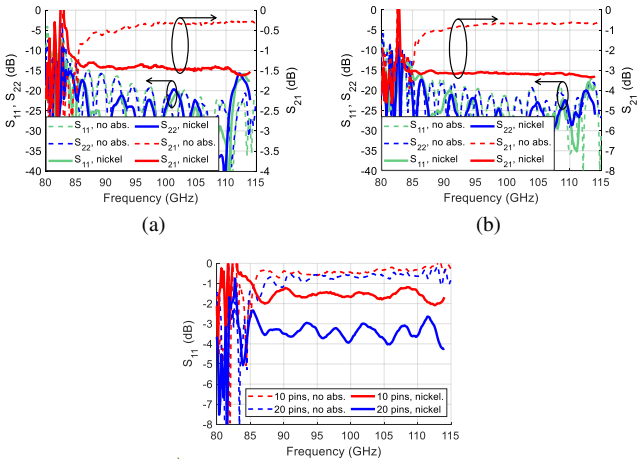

(a) (b)

(c)

Fig. 8. Comparison of measured S-parameters with and without the selective nickel plating: (a) 10-pin B2B structure; (b) 20-pin B2B structure; (c) OE structures.

C. Selective Nickel Plating

Nickel is a conductive ferromagnetic material, whose electromagnetic properties were comprehensively reported at low microwave frequencies [13], [14]. It was shown both theoretically and experimentally that a real part of nickel permeability (μ_r) approaches 1 around 10 GHz. A very limited information is available on nickel characterization at mm-wave and THz frequencies. In [15], the authors studied the effect of surface finish on antenna performance at V-band (60 GHz) reporting the increased dissipation for nickel-based design. This phenomenon was attributed to a moderate electrical conductivity of nickel that is noticeably lower as compared with copper and aluminum.

In this study, we likely for the first time experimentally investigated the effect of nickel plating on the waveguide transmission loss at high mm-wave frequencies. The test structures were selectively nickel-plated using commercial electroplating process (Fig. 7). The top metal plate of the RGWs was also selectively covered with nickel. The estimated

nickel thickness is around 5 μm that is sufficiently thicker than the skin depth at W-band. Measured results for all four test structures are presented in Fig. 8. The main observation is the increased insertion (for the B2B structures) and reflection (for the OE structures) loss. The measured insertion loss per unit length is approximately 2.5 dB/cm. An attempt was made to match the simulation model with measurements by tuning the nickel bulk electrical conductivity (σ). It was found that using $\sigma = 10^7$ S/m (*cf.* [13]), $R_q = 0.5$ μm, and $\mu_r = 1$ gives a noticeably smaller loss (around 1 dB/cm). Therefore, a further study on the nickel performance should be elaborated to reveal an origin of the high insertion loss.

The demonstrated performance of the nickel-plated RGW suggests its possible application for W-band fixed attenuators or narrowband (resonant) matched terminations. The latter implementations can be based on the coupled resonators concept.

IV. Conclusions

We have considered several methods of a regular RGW loading at W-band: (i) filling the air gap of the RGW with a carbon-loaded foam; (ii) covering the ridge (and pins) by a carbonyl iron paint; (iii) selective nickel plating of the RGW segment. Absorbing capabilities of the employed materials have been demonstrated experimentally. Summarizing the results, the following main conclusions can be drawn.

- Using the foam absorber is an inexpensive and convenient method for designing wideband well-matched RGW terminations. It is seen as an appropriate solution for creating low- to medium-power loads during laboratorial testing of RGW mm-wave circuits and array antenna measurements (e.g., for the embedded element pattern measurements).
- The carbonyl iron paint can be effectively used to create wideband RGW attenuators and terminations. Controlling the paint thickness is crucial for obtaining the required attenuation and good impedance matching. The method requires using a painting stencil and can be potentially employed for both laboratorial and industrial purposes. The power-handling capabilities of the method are yet to be investigated.
- The nickel-plated RGWs have demonstrated the insertion loss per unit length of 2.5 dB/cm. This value was found to be higher than expected based on the non-magnetic model of nickel. Whether the increased loss is attributed purely to a low electrical conductivity or there are yet some magnetic phenomena at W-band is still the question for future research. However, the revealed absorption performance of nickel suggests its application for creating mm-wave attenuators and resonant matched loads. The method can be interesting from the industrial perspective due to its high-power handling capabilities, good repeatability and durability.

Acknowledgment

This work has received funding from the European Union's Horizon 2020 research and innovation programme under the Marie Skłodowska-Curie grant agreement No 860023 and the Sweden-Taiwan Collaborative Research Framework Project "Antenna Technologies for Beyond-5G Wireless Communication" from the Swedish Foundation for Strategic Research.

References

[1] E. Rajo-Iglesias, M. Ferrando-Rocher, and A. U. Zaman, "Gap waveguide technology for millimeter-wave antenna systems," *IEEE Commun. Mag.*, vol. 56, no. 7, pp. 14–2, Jul. 2018.

[2] E. Alfonso, M. Baquero, P.-S. Kildal, A. Valero-Nogueira, E. Rajo-Iglesias, and J. I. Herranz, "Design of microwave circuits in ridge-gap waveguide technology," in *Proc. 2010 IEEE MTT-S International Microwave Symposium*, Anaheim, CA, USA, May 2010, pp. 1544–1547.

[3] M. Ivashina, A. Vilenskiy, H.-T. Chou, J. Oberhammer, and M. N. M. Kehn, "Antenna technologies for beyond-5G wireless communication: Challenges and opportunities," in *Proc. 2021 International Symposium on Antennas and (ISAP 2021)*, Taipei, Taiwan, Oct. 2021, pp. 1–2.

[4] P.-S. Kildal, E. Alfonso, A. Valero-Nogueira, and E. Rajo-Iglesias, "Local metamaterial-based waveguides in gaps between parallel metal plates," *IEEE Antennas Wireless Propag. Lett.*, vol. 8, pp. 84–87, 2009.

[5] Y. Zhang, A. R. Vilenskiy, and M. V. Ivashina, "W-band waveguide antenna elements for wideband and wide-scan array antenna applications for beyond 5G," in *Proc. 15th European Conference on Antennas and Propagation (EuCAP)*, Dusseldorf, Germany, Mar. 2021, pp. 1–5.

[6] T. Stander, P. van der Walt, P. Meyer, and W. Steyn, "A comparison of simple low-power wedge-type X-band waveguide absorbing load implementations," in *Proc. AFRICON 2007*, Windhoek, South Africa, Sep. 2007, pp. 1–3.

[7] Y. Naito and K. Suetake, "Application of ferrite to electromagnetic wave absorber and its characteristics," *IEEE Trans. Microw. Theory Techn.*, vol. 19, no. 1, pp. 65–72, Jan. 1971.

[8] Y. Zhang, Q. Wang, and J. Ding, "Short terminal load with broad bandwidth," *Electronics Letters*, vol. 49, no. 16, pp. 1–2, Aug. 2013.

[9] A. U. Zaman and P.-S. Kildal, "Wide-band slot antenna arrays with single-layer corporate-feed network in ridge gap waveguide technology," *IEEE Trans. Antennas Propag.*, vol. 62, no. 6, pp. 2992 – 3001, Jun. 2014.

[10] B. Zhao, M. Hamidinejad, C. Zhao, R. Li, S. Wang, Y. Kazemia, and C. B. Park, "A versatile foaming platform to fabricate polymer/carbon composites with high dielectric permittivity and ultra-low dielectric loss," *Journal of Materials Chemistry A*, vol. 7, pp. 133 – 140, 2019.

[11] L. de C. Folgueras, M. A. AlvesMirabel, and C. Rezende, "Microwave absorbing paints and sheets based on carbonyl iron and polyaniline: measurement and simulation of their properties," *Journal of Aerospace Technology and Management*, vol. 2, no. 1, pp. 63 – 70, 2010.

[12] Q. Yuchang, Z. Wancheng, J. Shu, L. Fa, and Z. Dongmei, "Microwave electromagnetic property of SiO_2-coated carbonyl iron particles with higher oxidation resistance," *Physica B: Condensed Matter*, vol. 406, no. 4, pp. 777–780, Feb. 2011.

[13] S. Lucyszyn, "Microwave characterization of nickel," *PIERS Online*, vol. 4, no. 6, pp. 686–690, 2008.

[14] S. N. Starostenko, K. N. Rozanov, A. O. Shiryaev, V. A. Garanov, and A. N. Lagarkov, "Permeability of nickel determined from microwave constitutive parameters of composites filled with nickel powders," *IEEE Trans. Magn.*, vol. 54, no. 11, pp. 1–5, Nov. 2018.

[15] E. Usta and N. T. Tokan, "Effects of surface finish material on millimeter-wave antenna performance," *IEEE Trans. Compon. Packag. Manuf. Technol.*, vol. 9, no. 5, pp. 815–821, May 2019.